JOURNAL OF THERMOPHYSICS AND HEAT TRANSFER
Vol. 7, No. 2, April–June 1993

Natural Convection Heat Transfer in a Three-Dimensional Duct

A. Moutsoglou* and M. R. Park†
South Dakota State University, Brookings, South Dakota 57007

A computational analysis is conducted to investigate the three-dimensional heat transfer and flow characteristics of laminar natural convection in a vertical duct, open to the ambient at the top and bottom and enclosed on all four sides. Detailed data are presented for air (Pr = 0.7) in a square duct heated/cooled isothermally or uniformly on one side with the remaining three walls assumed adiabatic. Numerical data are also obtained and presented for comparisons by way of a two-dimensional channel flow approximation. The channel flow model that neglects the slowing down of the streamwise velocities due to the friction of the lateral walls predicts considerably higher local and average Nusselt numbers than the three-dimensional analysis for a square duct. Present numerical results are compared to published experimental data. The numerical data are in good agreement with the experimental data of Elenbaas,[5] Wirtz and Stutzman,[7] and Sobel et al.,[8] but significantly underpredict the experimental data of Sparrow and Bahrami.[9]

Nomenclature

B = depth of the duct in the z direction, m
Gr_H = Grashof number based on the duct width, $g\beta|T_w - T_\infty|H^3/\nu^2$ for UWT, $g\beta|q_w|H^4/\nu^2 k$ for UHF
g = local gravitational acceleration, m/s^2
H = width of the duct in the y direction normal to heated/cooled wall, m
k = thermal conductivity, W/m-K
L = height of the duct in the x direction, m
$\overline{Nu}$ = average ambient Nusselt number, $Q_w H/kLB(\bar{T}_w - T_\infty)$
$\overline{Nu}_x$ = spanwise-averaged streamwise Nusselt number, $\bar{q}_x H/k(\bar{T}_{w,x} - T_\infty)$
P = dimensionless pressure
Pr = Prandtl number
p = pressure, Pa
Q_w = rate of heat transfer from heated/cooled surface to fluid, W
q_w = local heat flux from surface to fluid, W/m^2
$\bar{q}_x$ = spanwise-averaged streamwise heat flux from surface to fluid, W/m^2
T_b = bulk temperature, K
T_w = local wall temperature, K
$\bar{T}_w$ = average wall temperature of the heated/cooled surface, K
$\bar{T}_{w,x}$ = spanwise-averaged streamwise wall temperature, K
U, V, W = dimensionless velocity components
$\bar{U}$ = dimensionless average velocity, $\bar{u}H/\nu Gr_H$
u = streamwise velocity in x direction, m/s
$\bar{u}$ = average streamwise velocity, m/s
v = normal velocity in y direction, m/s
w = lateral velocity in z direction, m/s
X, Y, Z = dimensionless coordinates
x = streamwise coordinate, m
y = transverse coordinate, m
z = spanwise coordinate, m
α = thermal diffusivity, m^2/s
β = thermal expansion coefficient, K^{-1}
θ = dimensionless temperature, $(T - T_\infty)/(T_w - T_\infty)$ for UWT, $k(T - T_\infty)/q_w H$ for UHF
ν = kinematic viscosity, m^2/s
ρ = density, kg/m^3

Received Aug. 26, 1991; revision received March 10, 1992; accepted for publication April 23, 1992.

*Professor, Mechanical Engineering Department.
†Graduate Student, Mechanical Engineering Department.

Introduction

QUITE often, natural convection heat transfer in vertical open-ended rectangular ducts cannot be modeled as two-dimensional. For ducts that are heated or cooled at least at two or more adjacent sides, the flow and heat transfer are intrinsically three-dimensional. On the other hand, when two opposing sides of the duct are adiabatic and/or open to the ambient, and the heating or cooling incurs at the adjacent walls (one or both), the degree of three-dimensionality of the convection problem is strongly dependent on the duct depth-to-width ratio B/H. The duct depth B is defined as the interspace between the adiabatic and/or open sides, while H is the width in the direction normal to the heated/cooled side(s) (see Fig. 1).

The nature of induced flow in a duct with closed lateral edges is due to the chimney effect as the fluid is driven in the vertical direction by buoyancy-induced streamwise pressure gradients. When the lateral edges are open to ambient, the chimney effect subsides as fluid enters the duct from the open lateral edges due to spanwise pressure differences between the outside and inside of the duct. One may expect (as two-dimensional channel flow studies with finite-horizontal slits suggest[1,2]) the total flow leaving the duct in the vertical direction to be of the same order for ducts having closed or open lateral edges. The velocities of fluid drawn from the

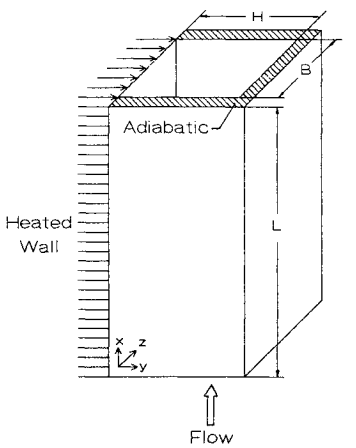

Fig. 1 Schematic of flow configuration and coordinate system.

open lateral edges of a duct with a fixed depth B are directly related to the duct width H. At low plate interspaces, the horizontal pressure imbalances are larger as the velocities of the fluid entering from the lateral edges become significant. On the other hand, as H increases, the velocities of the lateral flow are suppressed. Thus, along the edge, the flow boundary conditions resemble those for a closed wall, although the thermal boundary conditions may differ.

The existing computational studies on natural convection in vertical rectangular geometries are all limited to two-dimensional channel flows. Thus, they all model a duct with two adiabatic and/or open edges as being two-dimensional by assuming an infinite aspect ratio, i.e., $B/H \rightarrow \infty$. Various heating/cooling configurations were studied numerically for two-dimensional laminar-free convection channel flows. Bodoia and Osterle[3] analyzed a symmetrically heated channel for uniform wall temperature conditions. Aung et al.[4] presented numerical data for symmetrically and asymmetrically heated channels for both uniform wall temperature and uniform heat flux boundary conditions.

Any experimental data on natural convection from vertical parallel plates with either open or closed edges are, to a certain extent, inherently three-dimensional. All published experimental data on natural convection in vertical ducts are for heated (one or both) parallel plates, with either open to the ambient or unheated closed lateral edges. In Table 1 several of the published data and related conditions are summarized. As noted in Table 1, aside from the data of Elenbaas,[5] Sobel et al.,[8] and Sparrow and Bahrami,[9] the published data are geared towards verifying two-dimensional analyses as they pertain to relatively large depth-to-width ratios $B/H > 9.33$. In their experiments, Sparrow and Bahrami[9] used the naphthalene sublimation technique, which eliminates any radiation effects, extraneous convective/conductive heat losses, and variable property effects in obtaining average mass/heat transfer data for isothermal parallel vertical square plates ($L = B$). They attributed the large deviations between their data and those by Elenbaas[5] to overwhelming extraneous heat in the low range of $(H/L)Ra_H$ in Ref. 5, ($Ra_H = g\beta(T_w - T_\infty)H^3/\nu\alpha$), and to large unaccounted fluid property variations in Elenbaas'[5] data. Sparrow and Bahrami[9] commented on the inadequacy of $(H/L)Ra_H$ as a correlating parameter at small interplate spacings, and suggested that a three-dimensional model was in order at such instances. They showed that suppression of fluid along one lateral edge generally had only a modest effect on the average Nusselt numbers, and no effect when $(H/L)Ra_H > 4$. The largest decrease in average Nusselt numbers due to blockage of one lateral edge was less than 15% when $(H/L)Ra_H < 4$. They also found that when $(H/L)Ra_H > 10$, the lateral edge conditions do not effect the results, whereas, when both edges are blocked, 30% or more reductions in average Nusselt numbers are experienced at lower $(H/L)Ra_H$.

The effect of interplate spacing on natural convection in an open-ended vertical channel bounded by an isothermal and unheated wall was studied both experimentally and computationally by Sparrow and Azevedo.[11] Their data spanning from the limit of fully developed channel flow to the limit of single vertical plate demonstrated that single plate results do not form the upper bound for channel heat transfer rates. The experimental data for water ($Pr = 5$) were found to be correlated perfectly by a single, dimensionless parameter $(H/L)Ra_H$. They attributed this success to the absence of three-dimensional effects, even for relatively large spacings. It is worthwhile, however, to note that their data encompassed depth-to-width ratios of $13.3 < B/H < 66.6$ and are probably too large for three-dimensional effects to have any significant influence on heat transfer coefficients averaged over the entire heated plate, as indicated by the present study.

Since no prior study seems to exist in the literature, a computational analysis is conducted herein to investigate the three-dimensional flow and heat transfer characteristics of laminar natural convection in a heated or cooled vertical duct with enclosed sides. Numerical data are presented for air ($Pr = 0.7$) for various geometric duct configurations and heating conditions. Three-dimensional data are compared with corresponding two-dimensional data and single plate data to establish the accuracy and limitations of two-dimensional channel flow and single plate boundary-layer flow approximations.

Analysis

The present study focuses on the numerical prediction of buoyancy-induced laminar flow in a rectangular vertical duct. A schematic of the flow configuration and coordinate system is illustrated in Fig. 1. The duct is enclosed at all four sides and is open to ambient at the top and bottom. The duct is of finite height L, while having a width H (in the y direction) and depth B (in the z direction). The heating on one side of the duct is assumed to affect a uniform wall temperature (UWT) or a uniform heat flux (UHF) condition, while the remaining three sides are considered adiabatic. At the duct inlet, the buoyancy-driven flow is assumed to have an unknown uniform velocity $\bar{u}$, and be at the uniform ambient temperature T_∞. It is noted that even though the uniform inlet velocity assumption is quite reasonable at large B/H ratios, its validity is of concern at low B/H ratios.

In formulating the governing conservation equations, the fluid was taken to be incompressible with constant properties, while the Boussinesq approximation was utilized in modeling the buoyancy force. The three-dimensional Navier-Stokes and energy equations were parabolized by neglecting the axial diffusion of momentum and heat (terms involving $\partial^2/\partial x^2$), and secondly by decoupling the streamwise and lateral pressure gradients.[12] The local thermodynamic pressure $p(x, y, z)$ is therefore represented as the sum of a mean cross-sectional

Table 1 Experimental data in natural convection vertical ducts

Authors	Heating conditions	Edge conditions	B/H	L/H	Pr
Elenbaas[5]	Symmetric isothermal	Open to ambient	3–120	3–130	0.72
Levy et al.[6]	Symmetric isothermal	Open to ambient	12–48.8	15–61	0.72
Wirtz and Stutzman[7]	Symmetric uniform heat flux	Closed	17.1–38.2	17.1–38.2	0.72
Sobel et al.[8]	Symmetric uniform heat flux	Closed	6–12	2.3–10.5	0.72
Sparrow and Bahrami[9]	Symmetric isothermal	Open to ambient One edge open to ambient, one closed adiabatic Both closed adiabatic	2.4–3	2.4–3	2.5
Aung et al.[4]	Asymmetric isothermal	Closed	9.33–37.2	9.33–37.2	0.7
Sparrow et al.[10]	One wall isothermal, one wall adiabatic	Closed	10.1–15.2	15.2–22.9	5
Sparrow and Azevedo[11]	One wall isothermal, one wall adiabatic	Closed	13.3–66.6	20–100	5

pressure $\bar{p}(x)$ which drives the main flow, and a perturbation about the mean $\hat{p}(x, y, z)$. The decoupling further requires that $d\bar{p}/dx >> \partial\hat{p}/\partial x$.

The dimensionless governing system of equations for steady, laminar flow in a vertical duct can thus be expressed as

$$\frac{\partial U}{\partial X} + \frac{\partial V}{\partial Y} + \frac{\partial W}{\partial Z} = 0 \tag{1}$$

$$U\frac{\partial U}{\partial X} + V\frac{\partial U}{\partial Y} + W\frac{\partial U}{\partial Z} = -\frac{d\bar{P}}{dX} + \frac{\partial^2 U}{\partial Y^2} + \frac{\partial^2 U}{\partial Z^2} + \theta \tag{2}$$

$$U\frac{\partial V}{\partial X} + V\frac{\partial V}{\partial Y} + W\frac{\partial V}{\partial Z} = -\frac{\partial \hat{P}}{\partial Y} + \frac{\partial^2 V}{\partial Y^2} + \frac{\partial^2 V}{\partial Z^2} \tag{3}$$

$$U\frac{\partial W}{\partial X} + V\frac{\partial W}{\partial Y} + W\frac{\partial W}{\partial Z} = -\frac{\partial \hat{P}}{\partial Z} + \frac{\partial^2 W}{\partial Y^2} + \frac{\partial^2 W}{\partial Z^2} \tag{4}$$

$$U\frac{\partial \theta}{\partial X} + V\frac{\partial \theta}{\partial Y} + W\frac{\partial \theta}{\partial Z} = \frac{1}{Pr}\left(\frac{\partial^2 \theta}{\partial Y^2} + \frac{\partial^2 \theta}{\partial Z^2}\right) \tag{5}$$

The dimensionless variables appearing in the equations above are defined as follows:

$$X = \frac{x}{HGr_H}, \quad Y = \frac{y}{H}, \quad Z = \frac{z}{H}, \quad U = \frac{uH}{\nu Gr_H}$$

$$V = \frac{vH}{\nu}, \quad W = \frac{wH}{\nu}, \quad \bar{P} = \frac{(\bar{p} - p_\infty)H^2}{\rho\nu^2 Gr_H^2}, \quad \hat{P} = \frac{\hat{p}H^2}{\rho\nu^2} \tag{6}$$

where the mean dimensionless pressure $\bar{P}(X)$ is a measure of the local imbalance between the pressure within the duct and a corresponding ambient hydrostatic pressure $p_\infty(x)$ outside of the duct.

The dimensionless temperature θ appearing in Eqs. (2) and (5), and the Grashof number Gr_H used in Eq. (6) are dually defined, respectively, for UWT and UHF heating conditions:

$$\theta = \frac{T - T_\infty}{T_w - T_\infty}, \quad Gr_H = \frac{g\beta|T_w - T_\infty|H^3}{\nu^2} \quad \text{for UWT} \tag{7a}$$

$$\theta = \frac{k(T - T_\infty)}{q_w H}, \quad Gr_H = \frac{g\beta|q_w|H^4}{\nu^2 k} \quad \text{for UHF} \tag{7b}$$

The flow and thermal boundary conditions are specified as follows:

Inlet

$$U = \bar{U}, \quad V = W = \theta = 0, \quad \bar{P} = -\bar{U}^2/2 \quad \text{at} \quad X = 0 \tag{8a}$$

Exit

$$\bar{P} = 0 \quad \text{at} \quad X = L/HGr_H \tag{8b}$$

Sides

$$U = V = W = 0 \quad \text{at} \quad Y = 0, \; Y = 1$$

$$Z = 0, \quad Z = B/H \tag{8c}$$

$$\theta = 1 \quad \text{for UWT} \quad \text{or} \quad \frac{\partial \theta}{\partial Y} = -1 \quad \text{for UHF} \quad \text{at} \quad Y = 0 \tag{8d}$$

$$\frac{\partial \theta}{\partial Y} = 0 \quad \text{at} \quad Y = 1; \quad \frac{\partial \theta}{\partial Z} = 0 \quad \text{at} \quad Z = 0$$

$$Z = B/H \tag{8e}$$

where Bernoulli's equation is utilized in estimating the mean pressure at the inlet.

The dimensionless system of governing equations and boundary conditions [Eqs. (1–5) and (8)] are characterized by three dimensionless parameters: 1) the dimensionless duct height parameter L/HGr_H; 2) the cross-sectional aspect ratio B/H; and 3) the fluid Pr. It is also noted that the dimensionless system of equations describe both upward flow when the duct is being heated, or downward flow when the duct is being cooled. For the latter case, the origin of the coordinate system is at the top where the duct inlet is, and the axial coordinate is downwards in the direction of the gravity vector.

Computational Procedure

The governing system of differential Eqs. (1–5) and boundary conditions, Eq. (8), were solved using the control volume-based finite-difference scheme of Patankar and Spalding.[12]

From the parabolic nature of the equations, downstream events do not influence upstream conditions, and a marching procedure is employed. However, as the inlet duct velocity was treated as unknown (and assumed uniform), streamwise iterations by way of a Newton-Raphson scheme were necessitated in determining its value from the constraint of zero mean pressure imbalance at the exit. The Newton-Raphson iterations were ceased when the exit mean pressure was less than 0.01% of the maximum mean pressure inside the duct. The mean pressure gradient appearing in the streamwise X momentum [Eq. (2)] was determined from an overall mass conservation utilizing a Newton-Raphson scheme.

At each marching step, the elliptic problem resulting from the cross-stream momentum equations was solved using the SIMPLER algorithm of Patankar,[13] while employing a power law scheme in treating the convection-diffusion terms. Each set of resultant algebraic equations was solved using the tri-diagonal matrix algorithm by employing a double sweep for the pressure and pressure correction equations, and a single sweep for the remaining equations in cross-stream direction normal to the heated side (Y direction).

Extensive numerical experimentations were conducted in selecting the number and distribution of grid points as the grid interspacing varied in all three directions. In general, deviations between average ambient Nusselt numbers obtained with a mesh of 82 × 22 × 16 and 42 × 12 × 9 were less than 1% for the UHF case, and less than 8% for the UWT case. The Nusselt number data obtained with an 82 × 22 × 16 mesh were consistently lower than corresponding data that employed a mesh of 42 × 12 × 9. The corresponding deviations between the dimensionless average velocities obtained with a mesh of 82 × 22 × 16 and 42 × 12 × 9 were less than 3% for the UHF case, and less than 4% for the UWT case.

The presented numerical data employed 82 streamwise stations with increasing grid interspaces in the downstream direction to account for rapid streamwise variations of the velocity components and temperature near the inlet of the duct. Denser clustering of streamwise grid points near the inlet was employed at larger L/HGr_H parameters. A 22 × 16 cross-stream mesh was employed for the presented data. The grid interspaces in both Y and Z directions increased symmetrically from each wall to the center of the duct. Denser clustering of the transverse (Y direction) grid points was employed at lower L/HGr_H parameters.

The two-dimensional channel flow model employed an exactly analogous computational procedure to that described for the three-dimensional model. For the two-dimensional channel flow model, data are presented using a variable mesh of 162 streamwise and 82 cross-stream grid points. Channel flow data for average ambient Nusselt numbers using a mesh of 82 × 42 grid points exceeded corresponding data from the 162 × 82 mesh by less than 0.5 and 2% for the UHF and UWT cases, respectively. Corresponding deviations for the

dimensionless average velocities were less than 0.7 and 0.5% for the UHF and UWT cases.

Results

Data are presented for spanwise-averaged Nusselt numbers, streamwise- and spanwise-averaged Nusselt numbers, bulk temperatures, and dimensionless average velocities.

The spanwise-averaged ambient Nusselt numbers for the heated/cooled wall are defined from

$$\overline{Nu}_x = [\bar{q}_x/(\bar{T}_{w,x} - T_\infty)](H/k) \tag{9}$$

In Eq. (9), $\bar{q}_x$ and $\bar{T}_{w,x}$ represent the streamwise convective heat flux to the fluid and streamwise wall temperature, respectively, averaged in the spanwise direction of the heated/cooled wall:

$$\bar{q}_x = \frac{1}{B}\int_0^B q_w \, dz, \qquad \bar{T}_{w,x} = \frac{1}{B}\int_0^B T_w \, dz \tag{10}$$

Ambient Nusselt numbers averaged over the entire heated/cooled side are defined from

$$\overline{Nu} = \frac{Q_w}{LB(\bar{T}_w - T_\infty)}\frac{H}{k} \tag{11}$$

where Q_w is the total convective heat transfer rate from the heated/cooled side to the fluid, and $\bar{T}_w$ is the average surface temperature of the heated/cooled surface

$$Q_w = \int_0^L \int_0^B q_w \, dz \, dx, \qquad \bar{T}_w = \frac{1}{LB}\int_0^L \int_0^B T_w \, dz \, dx \tag{12}$$

The average velocity $\bar{u}$ and the local bulk temperature T_b are defined as

$$\bar{u} = \frac{1}{BH}\int_0^B \int_0^H u \, dy \, dz, \qquad T_b = \frac{1}{BH}\int_0^B \int_0^H \frac{u}{\bar{u}} T \, dy \, dz \tag{13}$$

For the two-dimensional channel flow model, no spanwise averaging is necessary in Eqs. (10), (12), and (13), as by definition, no parameter varies in the z direction for this case.

Present numerical data for a Prandtl number of 2.5 are compared to the experimental data of Sparrow and Bahrami[9] for a duct heated isothermally to the same uniform temperature along two parallel sides ($\theta = 1$ at $Y = 0$ and $Y = 1$), with closed adiabatic lateral edges ($\partial\theta/\partial Z = 0$ at $Z = 0$ and $Z = B/H$). Average Nusselt numbers for each plate based on heated interplate duct width and wall-to-ambient temperature difference as defined from Eq. (11) are shown in Table 2 for three geometric configurations along with corresponding data read from Fig. 6 of Ref. 9. In the same table, present two-dimensional channel flow data for the three L/HGr_H values are also indicated. The average Nusselt numbers estimated by the present three-dimensional model using a mesh of 82 × 22 × 16 are found to underpredict the experimental data[9] by about 13, 26, and 33%, respectively, at $L/HGr_H = 0.015$, 0.116, and 0.24. Most importantly, the Nusselt numbers estimated by the present two-dimensional flow model for $Pr = 2.5$ using a mesh of 162 × 82 are also shown to predict significantly lower Nusselt numbers than the experimental data.[9] This is unexpected, since for the enclosed duct with two adiabatic closed edges as B increases, the lateral edge wall effects of slowing down the fluid become less and less significant. This results in an increase of the average velocity and consequently larger Nusselt numbers. The two-dimensional approximation that models a duct with an infinite depth ($B \to \infty$) should provide an upper limit for the average velocity and Nusselt numbers in a duct with a fixed height L and width H that is being heated isothermally at the two (or one) parallel sides separated by the distance H. This trend is confirmed by the present data.

Present computational data for air in a duct with isothermally and symmetrically heated vertical parallel plates with blocked lateral edges are compared to the empirical data of Elenbaas.[5] In his study, Elenbaas[5] reports a correlation equation for his measurements, corrected so it can apply for plates which are infinitely long in the spanwise direction [Eq. (37) in Ref. 5]:

$$\frac{Q_w}{LB(T_w - T_\infty)}\frac{H}{k} = \frac{1}{24}\frac{Pr}{(L/HGr_H)} \cdot \{1 - \exp[-35L/HGr_H Pr]\}^{3/4} \tag{14}$$

The present two-dimensional computational data are in excellent agreement being within only 1% of the semiempirical data predicted from Eq. (14).

The present computational data are also compared with the experimental results of Wirtz and Stutzman[7] and those of Sobel et al.[8] that report data for natural convection between uniformly and symmetrically heated vertical parallel plates with blocked lateral edges. Present numerical data from the three-dimensional algorithm with $Pr = 0.708$, $B/H = 17.05$, and $L/HGr_H = 0.000293$ are compared with the empirical data presented in Fig. 5 of Ref. 7. The local spanwise-averaged wall temperature ratios $(\bar{T}_{w,x} - T_\infty)/(\bar{T}_{w,L} - T_\infty)$ predicted by the present three-dimensional computational model are consistently lower than the empirical data of Wirtz and Stutzman[7] for $Ra = 2414$ correlated by Eq. (4) and Table 2 of Ref. 7:

$$\frac{\bar{T}_{w,x} - T_\infty}{\bar{T}_{w,L} - T_\infty} = \left(\frac{x}{L}\right)^{0.3365} \tag{15}$$

The deviations range from 1% at $x/L = 0.1$, to 14% at $x/L = 1$. The relatively large deviations experienced near the exit of the duct are partly attributed to the omission of the radiation mode in the present computational model. With the uniform symmetric heating in the duct and the low emissivities ($\varepsilon \sim 0.2$) of the surfaces employed in Ref. 7, the radiation effects are practically absent for the majority of the channel except near the exit. Radiative cooling of the near-the-exit surfaces ($x/L > 0.8$) to the cooler surroundings has been

Table 2 Comparison of experimental data[9] with present numerical estimates for $Pr = 2.5$

(L/HGr_H)		(B/H)	$(\bar{u}H/\nu Gr_H)$	$[Q_w H/LB(T_w - T_\infty)k]$
0.015	Experiments[9]	3		2.48
0.015	Three-dimensional duct (present)	3	0.031	2.160
0.015	Two-dimensional channel (present)	∞	0.035	2.295
0.116	Experiments[9]	5		0.96
0.116	Three-dimensional duct (present)	5	0.06	0.710
0.116	Two-dimensional channel (present)	∞	0.066	0.744
0.24	Experiments[9]	6		0.60
0.24	Three-dimensional duct (present)	6	0.068	0.400
0.24	Two-dimensional channel (present)	∞	0.074	0.405

shown[14] to significantly reduce wall temperatures below the free convection values. At the relatively high aspect ratio of $B/H = 17.05$, the spanwise-averaged streamwise wall temperature predicted by the three-dimensional model were about 8% above those obtained by the present two-dimensional channel flow model.

The correlated data of Sobel et al.[8] at midheight temperatures, where radiative effects are not significant

$$\frac{q_w}{(\bar{T}_{w,L/2} - T_\infty)} \frac{H}{k} = 0.666 \left(\frac{Pr}{L/HGr_H}\right)^{0.2} \tag{16}$$

are found to agree exceptionally well with the present computational predictions. Thus, present two-dimensional data are found to be approximately only 3% higher than the data predicted from Eq. (16).

The data from the present two-dimensional channel flow model with $L/HGr_H = 0.00029$ were also compared with the two-dimensional numerical data of Aung et al.[4] presented in Fig. 7 of Ref. 4. To simulate the model used in Ref. 4, the present data for comparison were obtained by setting the mean pressure to be zero at the inlet. No differences in the two data could be detected from the figure.

Any presented data or discussion from here on pertain to an enclosed duct heated/cooled either isothermally (UWT) or at a uniform rate (UHF) on only one side ($Y = 0$). The remaining three sides ($Y = 1$, $Z = 0$, $Z = B/H$) are assumed to be adiabatic. The buoyancy-induced fluid is air with a Prandtl number of 0.7. Data were obtained at L/HGr_H values for each decade ranging from 10^{-3} to 1 for both UWT and UHF cases. For air, estimating the properties at 300 K, this corresponds to a range of pertinent parameters of about $1.3 \times 10^5\ \mathrm{m^{-3}K^{-1}} < L/H^4|T_w - T_\infty| < 1.3 \times 10^8\ \mathrm{m^{-3}K^{-1}}$ for the UWT case, and $4.9 \times 10^6\ \mathrm{m^{-2}W^{-1}} < L/H^5|q_w| < 4.9 \times 10^9\ \mathrm{m^{-2}W^{-1}}$ for the UHF case.

Nusselt numbers averaged over the entire heated/cooled side (Eq. 11) are illustrated for the uniform wall temperature (UWT) and uniform heat flux (UHF) conditions, respectively, in Figs. 2 and 3 for a square duct ($B/H = 1$) for air ($Pr = 0.7$).

Corresponding two-dimensional average channel Nusselt numbers obtained from the present study are also plotted in the same figures. Two-dimensional single plate data for an unbounded heated single plate ($H \to \infty$, $B \to \infty$) submerged in an infinite quiescent ambient fluid are also depicted in the same two figures. The data are obtained from similarity solutions for $Pr = 0.7$. The single plate ambient average Nusselt numbers, defined from Eq. (11), can be expressed as

$$\overline{Nu}_{sp} = \frac{0.4706}{(L/HGr_H)^{1/4}} \quad \text{for UWT}$$
$$\overline{Nu}_{sp} = \frac{0.5880}{(L/HGr_H)^{1/5}} \quad \text{for UHF} \tag{17}$$

First, reference is made to comparisons of average Nusselt number data between two-dimensional channel flow and two-dimensional single plate results. An inspection of Figs. 2 and 3 indicates the crossover of the two data near $L/HGr_H = 0.02$ for both UWT and UHF cases. It is reiterated that the Grashof numbers are defined differently (see Eqs. 7a and 7b) for the two heating conditions. For $L/HGr_H < 0.02$, the chimney effect due to the presence of the adiabatic wall is dominant and the resultant channel Nusselt numbers are higher than corresponding single plate data. For $L/HGr_H > 0.02$ on the other hand, as the flow and temperature become fully developed, the interaction of the thermal boundary layer with the adiabatic wall deteriorates the heat transfer. As a result, the channel Nusselt numbers dip below corresponding single plate data. For the UWT case (Fig. 2), eventually as L/HGr_H increases further, the fluid in the channel away from the inlet tends to attain the heated wall uniform temperature, and the channel Nusselt numbers approach zero. This is not so for the UHF case (Fig. 3), where the fluid temperature in the channel never attains the wall temperature and the Nusselt numbers are an inverse indication of the wall-to-ambient temperature difference.

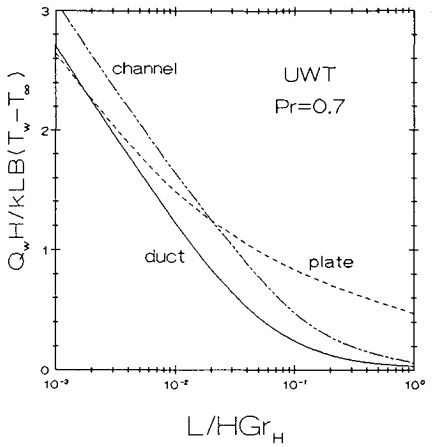

Fig. 2 Average Nusselt numbers for a vertical square duct heated/cooled isothermally on one side.

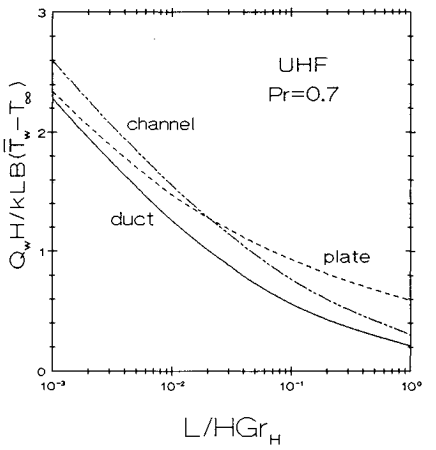

Fig. 3 Average Nusselt numbers for a vertical square duct heated/cooled uniformly on one side.

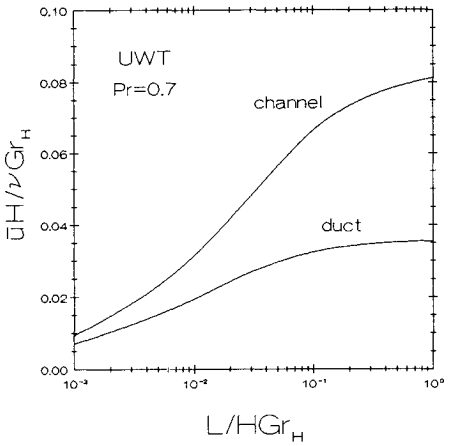

Fig. 4 Average velocities for a vertical square duct heated/cooled isothermally on one side.

Next, attention is drawn to the average Nusselt numbers for a duct with a square cross section ($B/H = 1$) and closed adiabatic edges. As can be seen from Figs. 2 and 3, the duct Nusselt numbers lie below the corresponding channel Nusselt numbers, as expected. This is due to the effects of the side walls restraining the flow, which results in lower duct average velocities (Figs. 4 and 5) and higher duct bulk temperatures

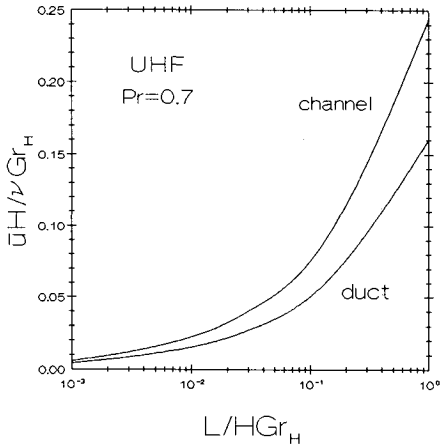

Fig. 5 Average velocities for a vertical square duct heated/cooled uniformly on one side.

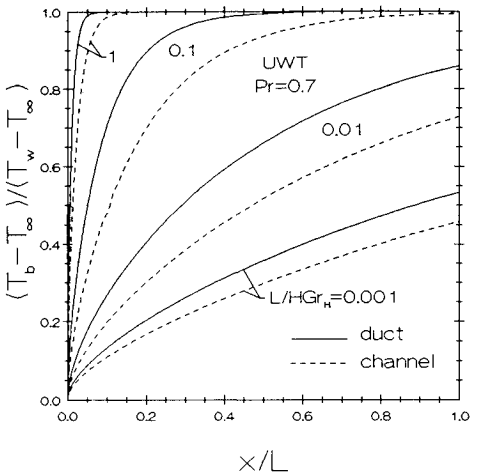

Fig. 6 Bulk temperatures for a vertical square duct heated/cooled isothermally on one side.

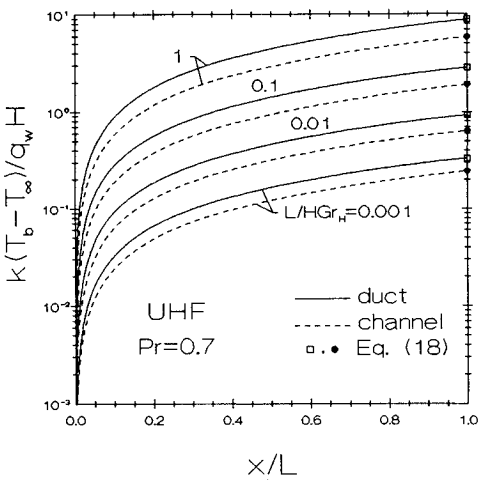

Fig. 7 Bulk temperatures for a vertical square duct heated/cooled uniformly on one side.

(Figs. 6 and 7) than corresponding channel flow data. Thus, for the UWT case, the channel flow approximation overestimates the average ambient Nusselt numbers for a square duct by about 14% over the value of 2.7 at $L/HGr_H = 10^{-3}$, and by about 109% above the value of 0.028 at $L/HGr_H = 1$. For the UHF case, the channel flow model overestimation is approximately 14% over the ambient duct Nusselt number value of 2.28 at $L/HGr_H = 10^{-3}$, and about 45% above the value of 0.208 at $L/HGr_H = 1$.

When the duct results are compared to single plate data, the crossover of the corresponding data in Figs. 2 and 3 shifts to lower L/HGr_H parameters. It is to be noted though, that the single plate data are for a plate of infinite depth ($B \rightarrow \infty$).

The dimensionless average velocities for a square duct ($B/H = 1$) and a corresponding channel heated on one side only are plotted in Figs. 4 and 5, respectively, for the uniform wall temperature and uniform heat flux conditions. As noted earlier, the effect of the adiabatic side walls of the duct is to reduce the local velocities in their vicinity, thus resulting in lower average velocities and flow rates than corresponding channel flow data. For the uniform wall temperature case (Fig. 4) the flow rate in the duct becomes choked when $L/HGr_H > 0.5$. This is because of the air attaining the uniform wall temperature in this range of parameters. For the corresponding channel flow, the choking is delayed until about $L/HGr_H > 3$, due to lower fluid temperatures resulting from increased average velocities for a channel. The choked average velocities of the channel are about 132% higher than the corresponding choked average velocities for a duct. On the other hand, for the uniform heat flux case (Fig. 5), no such choking is observed because the fluid temperature never attains the varying wall temperature and the average velocities increase continuously with L/HGr_H.

Although not shown here, the lower streamwise velocities encountered in the duct, as the scaling of the continuity equation suggests, result at lower normal velocities v than corresponding channel flow data. This, in turn, expedites the attainment of fully developed conditions resulting in shorter duct entry lengths than corresponding two-dimensional channel flow values. Also, the asymmetry in the magnitudes of v about the $y/H = 0.5$ plane, characteristic of the two-dimensional flow data for a channel heated only on one side, was replaced by the almost symmetric (in magnitude) corresponding duct profile. This is due to the damping effects of the duct edge walls.

The streamwise variation of the dimensionless bulk temperature for the two heating conditions are next illustrated, respectively, in Figs. 6 and 7. As the fluid is decelerated because of the presence of the side walls in the square duct, the fluid bulk temperatures exceed corresponding channel flow values throughout the height of the duct. For the uniform wall temperature case (Fig. 6), when L/HGr_H is of the order of 0.05, the air bulk temperature attains the uniform wall temperature near the exit of the duct. For the channel on the other hand, the bulk temperature of the air approaches the wall temperature at the exit when L/HGr_H is about 0.1. Thus, for UWT when $L/HGr_H > 1$ the heat transfer area is limited to a very small region near the inlet of the duct. For a corresponding channel, however, the active heat transfer area is somewhat longer due to higher velocities that occur in this case.

In Fig. 7, the square duct and channel bulk temperatures are plotted for prescribed uniform heat flux case. The accuracy of the computational scheme and soundness of the solution algorithm can be tested from an overall energy balance. Since the prescribed flux is uniform, the fluid bulk temperature should vary linearly with streamwise distance according to

$$\frac{k(T_b - T_\infty)}{q_w H} = \frac{(L/HGr_H)}{Pr} \frac{1}{\bar{U}} \frac{x}{L} \tag{18}$$

Using the corresponding computed values for the average velocities of the three-dimensional duct and two-dimensional channel, respectively, bulk temperatures at the exit ($x/L = 1$) evaluated analytically from Eq. (18) are also indicated in Fig. 7 using a square (□) for the duct, and a circle (●) for the channel. The largest errors, which occur at the exit plane, are of the order of less than 0.7% for a duct, and practically zero for a channel.

Next, attention is focused on the streamwise variation of Nusselt numbers averaged only over the depth of the duct B. The streamwise variation of these spanwise-averaged ambient Nusselt numbers, as defined from Eq. (9), is illustrated for a one-sided-heated square duct with uniform wall temperature and uniform heat flux conditions, respectively, in Figs. 8 and 9. In the same figures, corresponding Nusselt numbers based on H are also depicted for a two-dimensional channel, as well as for a two-dimensional single plate. The single plate similarity data are evaluated from

$$\overline{Nu}_{x,sp} = \frac{0.35295}{(L/HGr_H)^{1/4}} \frac{1}{(x/L)^{1/4}} \quad \text{for UWT}$$
$$\overline{Nu}_{x,sp} = \frac{0.49}{(L/HGr_H)^{1/5}} \frac{1}{(x/L)^{1/5}} \quad \text{for UHF} \tag{19}$$

As shown in the two figures, the spanwise-averaged Nusselt numbers vary quite drastically near the inlet but remain approximately constant throughout the remainder of the height for $L/HGr_H < 0.001$. For the UWT case in Fig. 8, as L/HGr_H increases, the air temperature attains the uniform surface temperature of the heated or cooled wall, and the duct and channel Nusselt numbers dive sharply to zero. This is not the case for the single plate data where an infinite constant temperature ambient fluid is assumed. The single plate Nusselt numbers, as shown in Figs. 8 and 9, remain approximately constant after the initial drop-off near the inlet for all dimensionless axial lengths, as dictated from Eq. (19).

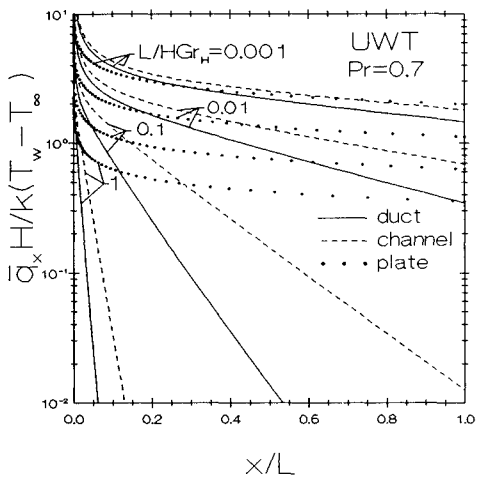

Fig. 8 Spanwise averaged ambient Nusselt numbers for a vertical square duct heated/cooled isothermally on one side.

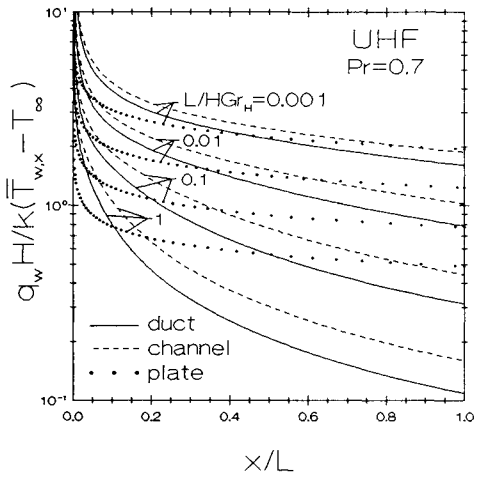

Fig. 9 Spanwise averaged ambient Nusselt numbers for a vertical square duct heated/cooled uniformly on one side.

The discussion of present data up to this point was concerned with a square duct ($B/H = 1$). The effects of the cross-sectional aspect ratio B/H on the flow and heat transfer characteristics of ducts enclosed on four sides and heated on only one side are demonstrated next. Nusselt numbers averaged over the entire heated side of the duct and based on the channel width H and ambient temperature are plotted in Fig. 10. The data correspond to both UWT and UHF conditions for $L/HGr_H = 0.01$. Average Nusselt numbers for corresponding channel flows based on interplate spacing H are also depicted as horizontal lines. As indicated by the figures, the average duct Nusselt numbers increase with increasing aspect ratio B/H due to the diminishing influence of the side walls and the resultant higher average velocities (see Fig. 11). With increasing B/H ratios, the duct average Nusselt numbers are shown to asymptotically attain their channel flow upper limit value. For the UWT case and with $L/HGr_H = 0.01$, the ambient average Nusselt numbers for a channel exceed corresponding duct Nusselt numbers by about 34, 13, and 1%, respectively, for cross-sectional aspect ratios of $B/H = 1$, 2, and 10. For the UHF case and with $L/HGr_H = 0.01$, the channel ambient average Nusselt numbers are approximately 24, 10, and 2% larger than corresponding ducts with $B/H = 1$, 2, and 10, respectively.

The cross-sectional effects of a duct on the dimensionless average velocities are illustrated in Fig. 11 for $L/HGr_H = 0.01$, for both uniform wall temperature and uniform heat flux conditions. As the aspect ratio B/H increases, the three-dimensional effects subside as the magnitude of the lateral velocities in the z direction diminishes, and the flow rates

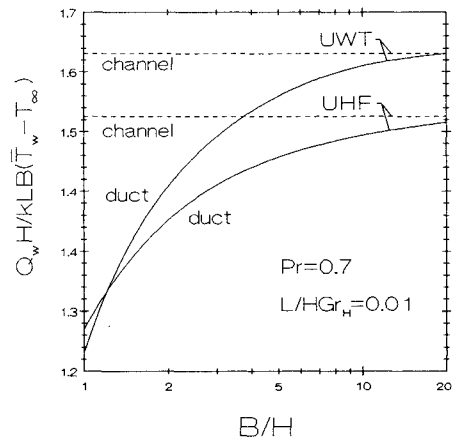

Fig. 10 Average Nusselt numbers for vertical ducts with different depth-to-width aspect ratios, heated/cooled isothermally or uniformly on one side.

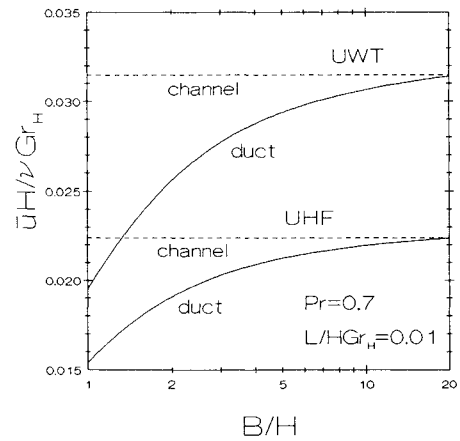

Fig. 11 Average velocities for vertical ducts with different depth-to-width aspect ratios, heated/cooled isothermally or uniformly on one side.

asymptotically attain their corresponding channel flow data. For the UWT case with $L/HGr_H = 0.01$, the flow rates predicted from a two-dimensional channel flow model exceed corresponding values predicted from a three-dimensional analysis by about 62, 23, and 3% for duct cross-sectional aspect ratios of $B/H = 1$, 2, and 10, respectively. For the UHF case with $L/HGr_H = 0.01$, the channel flow rates are approximately 46, 18, and 2% higher than ducts with $B/H = 1$, 2, and 10.

Summary

The degree of success of a two-dimensional channel flow model in predicting laminar natural convection in a vertical square duct is assessed by way of comparisons with computational data from a three-dimensional model. Data are presented for air ($Pr = 0.7$) in a one-sided heated/cooled square duct with a prescribed uniform temperature or uniform heat flux and the remaining three sides adiabatic. The channel flow model that neglects the flow restraining effects of the adiabatic lateral edges overestimates the heat transfer rates and the induced flow rates predicted by the three-dimensional flow model. The channel flow model is also found to overpredict the entry length region, while underestimating the axial location for the uniform wall temperature where choking occurs.

The present three-dimensional computational data compared quite well with the experimental data of Elenbaas,[5] Wirtz and Stutzman,[7] and Sobel et al.[8] Significant deviations, however, were encountered when the present data were compared with the experimental data of Sparrow and Bahrami.[9] Overall energy balances for the uniform heat flux case produced analytical exit bulk temperatures that matched corresponding computationally estimated values extremely well.

References

[1]Azevedo, L. F., and Sparrow, E. M., "Natural Convection in a Vertical Channel Vented to the Ambient Through an Aperture in the Channel Wall," *International Journal of Heat and Mass Transfer*, Vol. 29, June 1986, pp. 819–830.

[2]Moutsoglou, A., and Rhee, J. H., "Natural Convection-Radiation Cooling of a Vented Channel," *International Journal of Heat and Mass Transfer*, Vol. 35, Nov. 1992, pp. 2855–2863.

[3]Bodoia, J. R., and Osterle, J. F., "The Development of Free Convection Between Heated Vertical Plates," *Journal of Heat Transfer*, Vol. 84, Feb. 1962, pp. 40–44.

[4]Aung, W., Fletcher, L. S., and Sernas, V., "Developing Laminar Free Convection Between Vertical Flat Plates with Asymmetric Heating," *International Journal of Heat and Mass Transfer*, Vol. 15, Nov. 1972, pp. 2293–2308.

[5]Elenbaas, W., "Heat Dissipation of Parallel Plates by Free Convection," *Physica*, Vol. 9, Jan. 1942, pp. 1–28.

[6]Levy, E. K., Eichen, P. A., Cintani, W. R., and Shaw, R. R., "Optimum Plate Spacings for Laminar Natural Convection Heat Transfer from Parallel Vertical Isothermal Flat Plates: Experimental Verification," *Journal of Heat Transfer*, Vol. 97, Aug. 1975, pp. 474–476.

[7]Wirtz, R. A., and Stutzman, R. J., "Experiments on Free Convection Between Vertical Plates with Symmetric Heating," *Journal of Heat Transfer*, Vol. 104, Aug. 1982, pp. 501–507.

[8]Sobel, N., Landis, F., and Mueller, W. K., "Natural Convection Heat Transfer in Short Vertical Channels Including the Effects of Stagger," *Proceedings, Third International Heat Transfer Conference*, Vol. II, 1966, pp. 121–125.

[9]Sparrow, E. M., and Bahrami, P. A., "Experiments on Natural Convection from Vertical Parallel Plates with Either Open or Closed Edges," *Journal of Heat Transfer*, Vol. 102, May 1980, pp. 221–227.

[10]Sparrow, E. M., Chrysler, G. M., and Azevedo, L. F., "Observed Flow Reversals and Measured-Predicted Nusselt Numbers for Natural Convection in a One-Sided Heated Vertical Channel," *Journal of Heat Transfer*, Vol. 106, May 1984, pp. 325–332.

[11]Sparrow, E. M., and Azevedo, L. F., "Vertical-Channel Natural Convection Spanning Between the Fully-Developed Limit and the Single-Plate Boundary-Layer Limit," *International Journal of Heat and Mass Transfer*, Vol. 28, Oct. 1985, pp. 1847–1857.

[12]Patankar, S. V., and Spalding, D. B., "A Calculation Procedure for Heat, Mass and Momentum Transfer in Three-Dimensional Parabolic Flow," *International Journal of Heat and Mass Transfer*, Vol. 15, Oct. 1972, pp. 1787–1806.

[13]Patankar, S. V., *Numerical Heat Transfer and Fluid Flow*, Hemisphere, Washington, DC, 1980.

[14]Moutsoglou, A., and Wong, Y. H., "Convection-Radiation Interaction in Buoyancy-Induced Channel Flow," *Journal of Thermophysics and Heat Transfer*, Vol. 3, April 1989, pp. 175–181.